Thesis for The Degree of Licentiate of Philosophy

Atmospheric rivers in northern high latitudes and their impacts on the regional climate

Erik Holmgren

Department of Environmental and Energy Sciences
Chalmers University of Technology
Gothenburg, Sweden, 2026

Atmospheric rivers in northern high latitudes and their impacts on the regional climate

Erik Holmgren

Department of Environmental and Energy Sciences
Division of Geoscience and Remote sensing
Climate Dynamics Group
Chalmers University of Technology
SE-412 96 Göteborg,
Sweden
Phone: +46(0)31 772 1000

Cover: NASA Earth Observatory image by Jesse Allen and Joshua Stevens.
https://science.nasa.gov/earth/earth-observatory/river-in-the-sky-keeps-flowing-over-the-west-89700/

Printed by Chalmers Digitaltryck,
Gothenburg, Sweden 2026.

Atmospheric rivers in northern high latitudes and their impacts on the regional climate

Erik Holmgren

Department of Environmental and Energy Sciences
Chalmers University of Technology

Abstract

Atmospheric rivers (ARs) are long and narrow temporary pathways of unusually high and organized moisture transport in the lower troposphere. ARs have an important role in the global climate system as they facilitate a majority of the meridional moisture transport. This AR related moisture then stimulates regional weather patterns and is in many ways crucial for the local water supply in many regions. In the early days of the field, AR research primarily focused on local case studies over the west coast of North America. Today, while much of AR research remains focused on North America, studies on ARs and their interactions with the climate system now cover most regions of the world. For these studies, the level of detail typically decreases as the spatial scope increases. Hence, in recent years ARs over Europe have become relatively well studied. However, ARs over Scandinavia–and their impacts on the regional climate–have received limited scientific attention.

In this thesis I introduce a detailed climatology of ARs over Scandinavia. The study builds on the current state of global and regional AR research and leverages publicly available data from multiple AR detection algorithms to identify ARs that make landfall over Scandinavia. Using a clustering algorithm we could distinguish four different AR pathways through which ARs reach Scandinavia: a spatial level of detail not common for AR studies. We found that AR activity peaks over southern Denmark and the northern coast of Norway, with annual average frequencies reaching up to 4.2 % and 2.6 % respectively. Simultaneously, these regions receive up to 19.7 % and 13.1 % of their annual average precipitation during AR events. Furthermore, our use of multiple detection algorithms enables us to estimate the uncertainties in Scandinavian AR characteristics associated with algorithm choice.

This research serves as a robust foundation for future work focused on ARs over Scandinavia during the 21st century. Additionally, the novel clustering method can be applied to other regions, further uncovering how ARs impact regional climates.

Keywords

Atmospheric Rivers, Regional Climate, Precipitation, Scandinavia

Acknowledgment

I want to express my deepest appreciation to my supervisor, Hans Chen, for guiding me through the past years. Your knowledge and encouragement have been crucial to this work and my ongoing development as a researcher. You've kept me on track while at the same time given me plenty of freedom to explore my own ideas–which is vital in keeping doing science fun.

I also want to thank my fellow PhD students in the GEO corridor. Your dedication is an inspiration and I strive towards your curiosity. A conversation during lunch or an ice-cream in the sun, it always lightens a tough day.

Lastly, but definitely not least, I want to thank Gabriela for your constant support and belief in me, through all my ups and downs. I couldn't have got to this point without you.

List of Publications

Appended publications

This thesis is based on the following publications:

[**Paper I**] **E. Holmgren**, H. W. Chen, *A climatology of atmospheric rivers over Scandinavia and associated precipitation*
Weather and Climate Dynamics 39 (December 2025), 133-144.

Other publications

The following publications were published during my PhD studies, or are currently in submission/under revision. However, they are not appended to this thesis, due to contents overlapping that of appended publications or contents not related to the thesis.

[**a**] L. Ultee, F. Wimberly, S. Coats, J. Mackay, and **E. Holmgren**, *CMIP6 climate model spread outweighs glacier model spread in 21st-century drought buffering projections*
The Cryosphere, 20, , (February 2026), 1339–1361.

[**b**] F. Wimberly, L. Ultee, L. Schuster, M. Huss, D. R. Rounce, F. Maussion, S. Coats, J. Mackay, and **E. Holmgren**, *Inter-model differences in 21st century glacier runoff for the world's major river basins*
The Cryosphere, 19 (April 2025), 1491–1511.

[**c**] **E. Holmgren**, E. Kjellström, *Exploring the sensitivity of extreme event attribution of two recent extreme weather events in Sweden using long-running meteorological observations*
Nat. Hazards Earth Syst. Sci., 24 (August 2024), 2875–2893.

Contents

Abstract i

Acknowledgment iii

List of Publications v

Acronyms ix

I Summary 1

1 Introduction 3
1.1 What are atmospheric rivers? 3
1.2 Atmospheric rivers and modes of variability in the climate system 5
1.3 Physical mechanisms behind AR impacts 7

2 Climatology and impacts of atmospheric rivers around the world 11
2.1 Global impacts of atmospheric rivers on weather and climate . 11
2.2 Atmospheric rivers at high latitudes 12
2.3 Atmospheric rivers over Scandinavia 13

3 Common datasets and detection of atmospheric rivers 15
3.1 Reanalysis products 15
3.2 Climate model output 16
3.3 Detecting and tracking atmospheric rivers 18
3.3.1 AR detection algorithms 18
3.4 An overview of the Atmospheric River Tracking Method Intercomparison Project 23

4 Summary of included papers and future work 27
4.1 Paper 1: A climatology of atmospheric rivers over Scandinavia and associated precipitation 27
4.2 Future work 29

Bibliography 31

II Appended Papers 41

Paper I - A climatology of atmospheric rivers over Scandinavia and associated precipitation

Acronyms

AO Arctic Oscillation.

AR Atmospheric River.

ARDT Atmospheric River Detection and Tracking algorithm.

ARTMIP Atmospheric River Tracking Method Intercomparison Project.

CAM5 Community Atmosphere Model, version 5.

CMIP Coupled Model Intercomparison Project.

CMIP5 Coupled Model Intercomparison Project Phase 5.

CMIP6 Coupled Model Intercomparison Project Phase 6.

ECMWF European Center for Medium-range Weather Forecasts.

ENSO El Niño Southern Oscillation.

EOF Empirical Orthogonal Function.

ERA-Interim ECMWF Reanalysis Interim.

ERA5 ECMWF Reanalysis v5.

GHG Greenhouse Gas.

GMAO Global Modeling and Assimilation Office.

IPCC Intergovernmental Panel on Climate Change.

IVT Integrated water Vapour Transport.

IWV Integrated Water Vapour.

JMA Japanese Meteorological Agency.

JRA-55 Japanese 55-year Reanalysis.

LLJ Low-Level Jet.

MERRA-2 Modern Era Retrospective analysis for Research and Applications, version 2.

MIP Model Intercomparison.

NAO North Atlantic Oscillation.

RCP Representative Concentration Pathway.

SLP Sea Level Pressure.

SSP Shared Socioeconomic Pathway.

SST Sea Surface Temperature.

WCB Warm Conveyor Belt.

WCRP World Climate Research Programme.

WMO World Meteorological Organization.

Part I

Summary

Chapter 1

Introduction

1.1 What are atmospheric rivers?

The global hydrological cycle describes the processes through which water is continuously recirculated among the oceans, atmosphere, and land. One of the processes that redistributes moisture evaporated from the oceans is the phenomenon known as Atmospheric Rivers (ARs). ARs are long, but narrow, filaments of unusually high and organized moisture transport in the lower troposphere (e.g. Newell et al., 1992; Zhu & Newell, 1998). See Fig. 1.1 for an illustration. ARs are estimated to account for a majority of the global meridional moisture transport in the extratropical and polar atmosphere, while their combined widths occupy up to 10 % of the total longitudinal length at any given latitude (e.g. Nash et al., 2018; Zhu & Newell, 1998). Furthermore, ARs are important for the hydroclimate of many regions (e.g. Gimeno et al., 2014).

To understand the setting and formation of ARs, we have to start with extratropical cyclones. Extratropical cyclones form poleward of 30° latitude (N/S) in the lower troposphere. These localized low-pressure systems are characterized by horizontal winds that circulate in the same direction as the local vertical component of the planetary rotation; counterclockwise on the Northern Hemisphere and clockwise on the Southern Hemisphere (e.g. North et al., 2015). An extratropical cyclone begins as a disturbance in the upper levels of the troposphere, in the vicinity of the extratropical jet streams. With time, this disturbance propagates down into the lower troposphere which creates a low pressure region. As the cyclone continues to draw energy from the upper level disturbance it will continue to deepen, and air masses will move towards the increasingly low pressure: relatively warmer air will move poleward towards the system, while relatively colder air will move equatorwards. These air masses, and the leading edges specifically, create the warm- and cold-fronts associated with the advancing cyclone. Ahead of the cold front(s), on the warmer side, a strong air mass transport emerges which is known as the warm conveyor belt (WCB). Climatologically WCBs of extratropical cyclones play a key role in the poleward transport of sensible and latent heat (e.g. Browning, 1990). In the

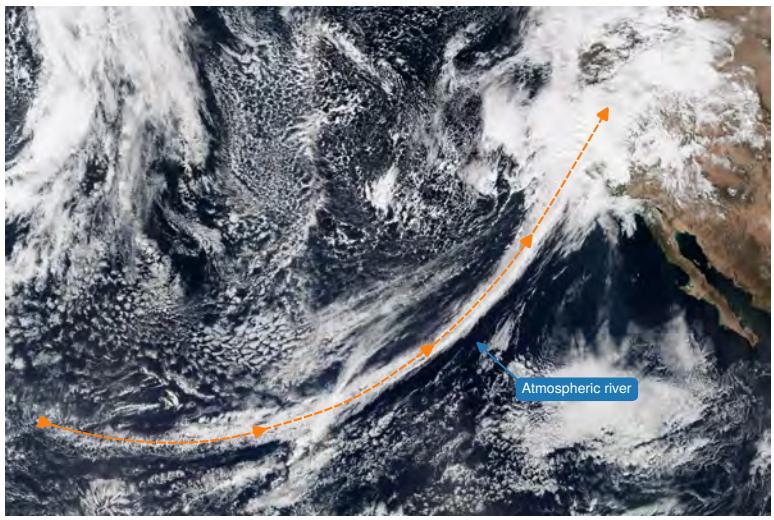

Figure 1.1: Satellite image of an AR over the north Pacific that makes landfall over the west coast of the USA. Orange, dashed, AR axis is approximate. Image adapted from the NASA Earth Observatory.

WCB, the strong temperature gradient can give rise to a low-level jet (LLJ) which strengthens the advection of water vapour along the front. Additionally, frontal convergence can force the air to ascend which further enhances the specific humidity locally. It is in these pre-frontal regions of extratropical cyclones that ARs form (Ralph et al., 2004, 2005), which serve as an additional conceptual model for moisture transport (H. Dacre, 2020). Fig. 1.2 shows a conceptual mesoscale view of an AR, including the associated cold front(s) and the LLJ introduced above.

The name "atmospheric rivers" implies a long range transport of water far from the regions where the water eventually rains out. However, as with regular rivers, moisture can enter and exit the stream along the way, and complex mechanisms regulate how much of the moisture within an AR comes from remote and local sources. The early theoretical definition of ARs began as an additional mechanism to the global moisture redistribution, which at the time was considered mostly eddy-driven. The river-like mechanism was proposed to highlight the filamentary structures observed in fields of atmospheric moisture transport (e.g. Zhu & Newell, 1998). Today, research on moisture sources of atmospheric rivers is still ongoing, with continued scientific discourse on how much of AR moisture comes from local or remote sources. The methods investigating remote sources generally use Lagrangian trajectories to backtrack and identify the source regions of moisture in landfalling ARs. This category of studies shows that landfalling ARs source most of their moisture further upstream over ocean basins (e.g. LeGrande et al., 2024; Sodemann & Stohl, 2013; Stohl et al., 2008). AR-related precipitation at mid and high latitudes also exhibits a time-lagged relationship with regions of anomalous moisture uptake

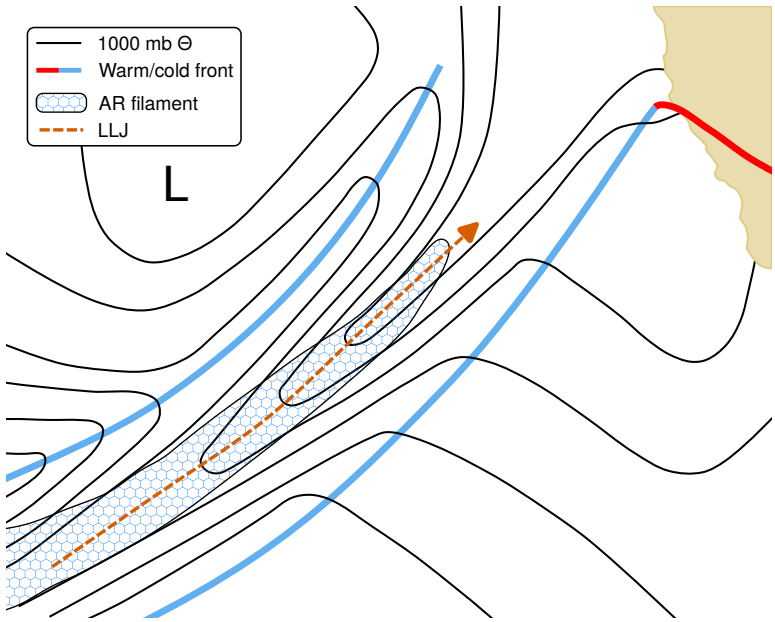

Figure 1.2: Conceptual figure of the mesoscale view of an AR. Black solid lines show the 1000 mb potential temperature surface, thick blue (red) lines cold (warm) fronts, and the dashed orange line the pre-frontal low-level jet. The blue patterned area indicate an AR filament. Figure adapted from Ralph et al. (2004).

in the subtropics and tropics (Ramos et al., 2016). Additionally, compared to the non-AR climatology, ARs appear to reduce both evaporation and heat fluxes from the ocean directly beneath them (LeGrande et al., 2024). In contrast, other studies (e.g. Bao et al., 2006; Sodemann & Stohl, 2013) have found that local sources of moistures and heat have an equal, if not more, important role than remote sources in AR moisture supply. Specifically, the high moisture content in ARs is a result of local moisture convergence driven by cyclogenesis (Bao et al., 2006; H. F. Dacre et al., 2015). Hence, the question of AR moisture sources remains contested.

1.2 Atmospheric rivers and modes of variability in the climate system

The inherent variability of the climate system exhibits large-scale reoccurring patterns in both space and time. These patterns are known as modes of variability (IPCC, 2023). Modes of variability are driven by the complex dynamics of atmospheric circulation, at times through coupled processes between the ocean and the atmosphere, and occasionally through interactions with land

surfaces and sea ice. These modes are typically described by an oscillation of one or multiple climate variables, such as Sea Surface Temperature (SST) or Sea Level Pressure (SLP), that vary on timescales ranging from daily, through seasonal, to multi-decadal. While a mode of variability usually coincides with variations in the local weather and climate, ARs are no exception, their effects often extend over much of the planet through so called teleconnections. Teleconnections refers to how different climate variables can be linked over large distances (1000s km). Methods used to detect and describe modes of variability include both simple techniques that look for covariance in the spatial means of predefined regions, and more sophisticated approaches that use Empirical Orthogonal Functions (EOFs) to identify covarying patterns in gridded climate variables.

One well known mode of variability is the North Atlantic Oscillation (NAO). The NAO is the major pattern of atmospheric variability over the North Atlantic. It appears as a seesaw (oscillation) in the SLP difference between the semi-permanent high pressure over the Azores and the semi-permanent low pressure over Iceland (see Fig. 1.3; e.g. Hurrell et al., 2003). The NAO is said to be in a positive phase when the SLP difference is stronger than usual, while the SLP difference is weaker than usual during a negative phase. Variations in the NAO coincide with large-scale changes in the atmospheric circulation over the Northern Hemisphere, which in turn affect surface temperatures over North America, Northern Europe and Asia, and the North Atlantic (Hurrell & Deser, 2010), as well as moisture transport and the ensuing precipitation in the North Atlantic region (Hurrell, 1995). The NAO has been shown to modulate AR activity over much of the Northern Hemisphere. During negative phases of the NAO, Southern Europe experiences higher than usual AR activity. For Northern Europe the apparent relationship is reversed, and AR activity increases during positive phases of the NAO (Lavers & Villarini, 2013). In contrast, it has also been shown that the NAO does not correlate with AR activity over the Iberian Peninsula (Ramos et al., 2015). An alternative approach is to use different weather regimes as a more detailed method to categorize how large-scale atmospheric circulation modulates AR activity (e.g. Lavers et al., 2012; Pasquier et al., 2019).

The NAO is in turn strongly correlated to, and essentially a subset of, another mode of variability: the Arctic Oscillation (AO). The AO describes the seesaw pattern in the within-Arctic and outside-Arctic SLP anomalies (see Fig. 1.3) and is well correlated to the strength of the polar jet stream (Thompson & Wallace, 1998). During the negative phases of the AO the seesaw exhibits positive anomalies within the Arctic and negative anomalies outside the Arctic, resulting in a weaker polar jet. During the negative phases, AR frequencies are lower than usual in e.g. Northern Europe while ARs are more common in subtropical regions of the North Atlantic, the Pacific of western U.S., and Southern Europe. On the other hand, during the positive phases of the AO, which coincide with a stronger-than-usual polar jet, AR frequency anomalies are reversed, with enhanced AR activity over Northern Europe (Guan & Waliser, 2015).

The El Niño Southern Oscillation (ENSO) is a major mode of variability

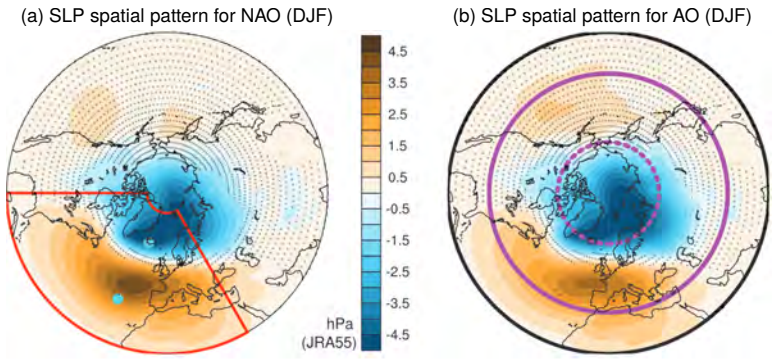

Figure 1.3: Leading EOF patterns of SLP anomalies for (a) NAO and (b) AO during December–February. Cyan circles in panel (**a**) indicate locations of low and high pressure centres for the NAO. The within-Arctic low-pressure of the AO is within the dashed purple line in panel (**b**). Figure adapted from IPCC (2023).

that captures the interannual alterations of SSTs in the equatorial Pacific (see Fig. 1.4; e.g. Philander, 1983). While ENSO is local to the tropical Pacific, it influences weather all over the world through climatic teleconnections (IPCC, 2023). There are two named phases, or events, of the ENSO: El Niño and La Niña. During El Niño the central and eastern equatorial Pacific exhibits higher than usual SSTs, weaker east to west SLP gradients, westerly winds anomalies, and increased precipitation. La Niña events instead exhibits lower than usual SSTs in the central and eastern parts of the equatorial Pacific, stronger gradients in SLP, and anomalous easterly surface winds. The influence of ENSO on ARs is limited, but also underexplored. ARs have been shown to increase (decrease) during El Niño (La Niña) conditions in some subtropical and extratropical regions, namely in the northern Pacific, North Atlantic, and the Gulf of Mexico (Guan & Waliser, 2015; Ralph et al., 2005).

1.3 Physical mechanisms behind AR impacts

ARs influence the surrounding weather and climate through the transport of two quantities: large amounts of moisture and energy. The moisture transported by ARs take part in processes where, in the end, the moisture reaches the ground and contributes to the water balance of the region: it precipitates, either through rain- or snowfall. This is especially common when ARs encounter steep topography (e.g. mountains) which forces the moist air to ascend, which often causes heavy orographic precipitation (e.g. Gimeno et al., 2014; Neiman et al., 2008; Stohl et al., 2008). AR precipitation is also, to a smaller extent, induced by frontal and convective processes (e.g. Ralph et al., 2011). The effects of AR-related precipitation can be considered double-edged as it both contributes to and sustains the water balance in many regions, but at the same

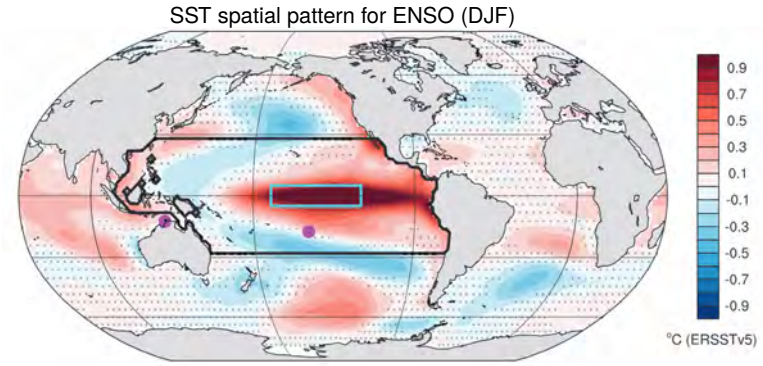

Figure 1.4: Spatial SST pattern for ENSO in December–February. ENSO can be defined as the average of SST anomalies in the cyan box, or by the EOF over the area denoted by the black line. Figure adapted from IPCC (2023).

time AR related heavy precipitation also causes severe flooding (Paltan et al., 2017). Figure 1.5 shows a conceptual overview of AR-related processes in the atmosphere.

Inherently through their high moisture (or water vapour) content, ARs transport large amounts of energy in the form of sensible and latent heat (e.g. Shields et al., 2019). The sensible heat has direct effects on the local energy balance, as turbulent mixing towards the surface extracts the energy from the AR, heating the surrounding atmosphere. The latent heat of the AR is contained within the water vapour, and is made available when the water vapour condenses to cloud droplets or precipitation. This process releases additional energy into the surrounding atmosphere, raising temperatures further (e.g. Kump et al., 2014). The elevated water moisture content of the atmosphere also contributes to an increased blockage of outgoing long-wave radiation, either directly or by contributing to an increased cloud cover, further increasing the temperatures in the area surrounding the AR.

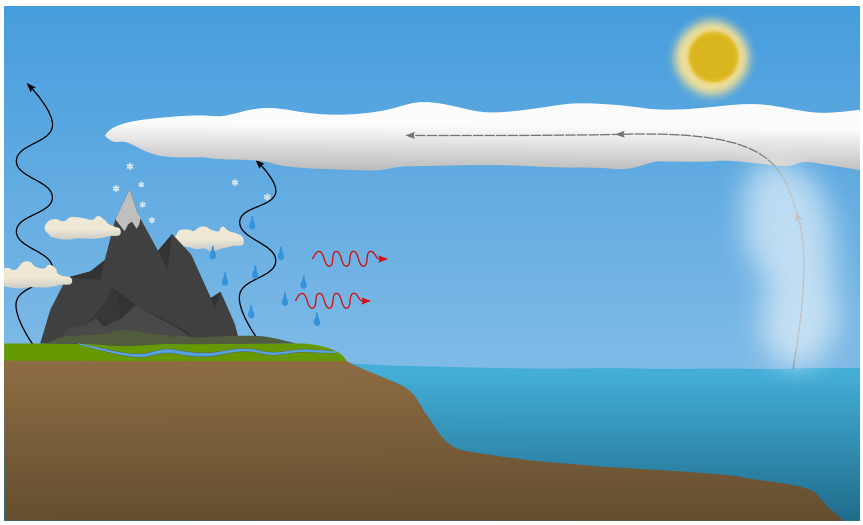

Figure 1.5: Conceptual figure showing AR related atmospheric processes. Moisture evaporates over the ocean and is transported towards and in over land (dashed arrow). The moisture precipitates as rain and snow, releasing latent heat (red arrows). Long wave radiation (black arrows) is hindered by the increased moisture content.

Chapter 2

Climatology and impacts of atmospheric rivers around the world

2.1 Global impacts of atmospheric rivers on weather and climate

ARs are an established feature in the local weather and climate of many midlatitude regions. Early AR research was mostly focused on case studies over the North American region, typically along the west coast of the United States (e.g. Ralph et al., 2004, 2005), demonstrating the theoretical definition of ARs from Zhu and Newell (1998). More recent climatologies establish that ARs are present for up to 13 % of the time annually along the west coast of the United States, with a slight prevalence for winter (November–March; Guan and Waliser, 2019; Rutz et al., 2014). These ARs are associated with up to 50 % of the wet-season (November–April) precipitation (e.g., Dettinger et al., 2011; Guan & Waliser, 2015; Rutz & Steenburgh, 2012). AR-related precipitation events have also been linked to ending persistent droughts in the region (Dettinger, 2013), as well as causing floods (Ralph et al., 2006).

However, ARs are a global phenomenon, and in the last decades the interest for ARs has spread outside of North America. Southern, Southeast, and East Asia experience up to 36, 32, and 24 AR days per year on average, respectively (Liang & Yong, 2021). ARs in South and East Asia are most frequent during the summer months, while Southeast Asia experiences most ARs during autumn and winter. Over the more coastal regions of East Asia, ARs are related to up to 44 % of the precipitation during spring through autumn (Kamae et al., 2017), while ARs contribute up to 32 % to the annual precipitation in South Asia (Liang & Yong, 2021). Interestingly, in East Asia, ARs in the northern areas show a significant decreasing trend between 1951–2015, while at the same time AR activity has been increasing in the southern regions (Liang

et al., 2023). Furthermore, ARs over Asia have been linked to more than 50 % of precipitation amounts during extreme precipitation events (Kim et al., 2021; Liang & Yong, 2021), and have been associated with up to 70 % of precipitation during the early stages of the East Asian summer monsoon (Park et al., 2021). On the other hand, ARs in the Bay of Bengal are instead more strongly associated with winter precipitation (Yang et al., 2018).

In Western Europe, the annual AR activity is of a similar magnitude to that of North America. Here, annual AR frequencies reach 13 % along the European Atlantic coastline: the British Isles, parts of Norway, Spain, and Portugal (Guan & Waliser, 2019). In these regions the AR-related precipitation contributes up to 30 % of the annual total precipitation, mostly during autumn and winter (Lavers & Villarini, 2015). ARs over Europe have been linked to many of the strongest annual precipitation events (Lavers & Villarini, 2013), heavy winter floods in Britain (Lavers et al., 2012), intensive precipitation in the Netherlands (van der Breggen & Hudson, 2024), and some of the largest floods in the lower Rhine basin (Ionita et al., 2020). Furthermore, precipitation amounts during flood events in northwestern Spain have been shows to double in the presence of ARs, no matter the synoptic conditions (Eiras-Barca et al., 2018).

Although currently less studied, ARs have a role in the hydroclimate of many other regions of the world. During the austral winter months (May–September) between 1979–2014, the west coast of South Africa experienced 10–15 AR days on average, with AR associated precipitation contributing 15–60 % of the winter total (Blamey et al., 2018). Along the west coast of South America ARs make landfall between 35–40 days per year, while contributing 40–60 % of the annual precipitation (Viale et al., 2018). Additionally, in the Southern Alps of New Zealand ARs have a strong influence on the largest floodings (Kingston et al., 2016) and during events of extremely high glacial ablation and snowfall (Little et al., 2019).

2.2 Atmospheric rivers at high latitudes

The role of ARs in regional weather and climate is not limited to the midlatitudes, and extends to high latitude regions. Over Antarctica ARs make landfall 3–10 days per year, and despite this relatively low frequency, they contribute to 10–20 % of the annual snowfall (Maclennan et al., 2023; Wille et al., 2021). Additionally, anomalously high snowfall events have been associated with ARs (Gorodetskaya et al., 2023; Wille et al., 2021). On other hand, ARs are also strongly linked to record-breaking high temperatures and surface melt on the Antarctic peninsula (Gorodetskaya et al., 2023) and in East Antarctica (Wille et al., 2024a, 2024b). The AR driven influences on the surface energy balance mainly act through increased downward long-wave radiation (e.g. Gorodetskaya et al., 2023). ARs have also been shown to indirectly increase short-wave radiation through their effects on foehn winds. An AR reaching the leeward slope of the foehn releases additional latent heat, strengthening the foehn and the subsequent foehn clearance on the windward side (Zou et al., 2023). Moreover,

strong ARs over the Antarctic peninsula precluded the main collapses of the Larsen A and B ice shelves in 1995 and 2002 respectively, and were found to have preceded 60 % of calving events taking place between 2000–2020 (Wille et al., 2022).

Arctic ARs are important for land-surface processes in Greenland, northern Canada, and northern Russia, and play a crucial role in the seasonal cycle of sea ice. Overall, Arctic ARs are associated with 40 % of summer precipitation (generally snowfall), and almost all rainfall during both spring and summer (Lauer et al., 2023). And while AR-induced snowfall contributes positively to the winter surface mass balance of the Greenland ice sheet, these gains are outweighed by summer-season surface melt, caused either directly by ARs (Mattingly et al., 2018), or indirectly from AR-induced foehn winds (Mattingly et al., 2023). Furthermore, the moisture transported by ARs to the Arctic significantly slow sea ice growth (Li et al., 2024; Zhang et al., 2023), which accounts for 34 % of the decline in early winter sea ice cover (Zhang et al., 2023).

2.3 Atmospheric rivers over Scandinavia

ARs over Scandinavia, which the paper part of this thesis examines, have previously received limited scientific attention. Most of the prior research on ARs over Scandinavia has focused on local extreme precipitation events and how they are related to ARs. Stohl et al. (2008) investigated one particularly extreme precipitation event over the southwest coast of Norway and how it might be linked to ARs. They used Lagrangian trajectories based on the moisture precipitating in the event and showed that moisture was sourced through evaporation in the middle of the North Atlantic Ocean. The moisture was subsequently funnelled into a narrow stream, or AR, towards Norway by two extratropical cyclones.

Continuing on the theme of extreme precipitation, Azad and Sorteberg (2017) used satellite measurements of IWV and in-situ precipitation measurements to conclude that 19 out of 20 extreme daily precipitation events in Norway between 1989–2009 where related to ARs. Additionally, for heavy cold season precipitation, up to 85 % of events over Norway between 1979–2014 are linked to ARs (Benedict et al., 2019). Although these studies use different datasets and employ different definitions of ARs, they both anchor the role of ARs in extreme precipitation over Norway. Regarding future changes, a single model climate projection shows that ARs over Norway will become more frequent and intense by the end of the 21st century, especially during late summer and autumn (Whan et al., 2020).

Chapter 3

Common datasets and detection of atmospheric rivers

Just as there are many algorithms used to detect and track atmospheric rivers, there are different groups of datasets used for said detection. This chapter includes brief descriptions of the two common classes of datasets used in AR detection, a general overview of Atmospheric River Detection and Tracking algorithms (ARDTs) and how they work, followed by a detailed description of the ARDTs I have used in my research. The chapter ends with a presentation of the Atmospheric River Tracking Method Intercomparison Project (ARTMIP) and a summary of their findings.

3.1 Reanalysis products

Reanalysis products are gridded datasets of weather related variables describing the state of for instance the atmosphere or the ocean. A reanalysis product usually spans multiple decades at a temporal resolution on the order of hours, while simultaneously having a relatively high continuos spatial resolution in both the horizontal and vertical domain. These "maps without gaps" are produced by assimilating archived weather observations while re-running modern weather forecasting systems over a period that has already been observed. For numerical weather models, assimilation aims to continuously correct the short term forecasts by adjusting forecasted variables towards their observed state. The assimilation enables the model to combine and relate different observations from multiple sources when computing the state of the atmosphere. This differs from traditional methods used for processing observations into gridded products, which commonly relies on spatio-statistical relationships to fill the missing gaps between the observations.

Reanalysis products are widely used in atmospheric and climate sciences, and are routinely used by both the WMO and the IPCC in their assessments

of the current climate (Hersbach et al., 2020). Numerous weather agencies and research institutes produce reanalysis products, with some of the more well known products listed in Table 3.1.

Table 3.1: Overview of selected reanalysis products mentined in this thesis.

Agency	**Acronym**	**Full Name**	**Source**
European Center for Medium-range Weather Forecasts (ECMWF)	ERA5	ECMWF Reanalysis v5	Hersbach et al. (2020)
	ERA-Interim	ECMWF Reanalysis Interim	Dee et al. (2011)
Global Modeling and Assimilation Office (GMAO)	MERRA-2	Modern Era Retrospective analysis for Research and Applications, version 2	Gelaro et al. (2017)
Japanese Meteorological Agency (JMA)	JRA-55	Japanese 55-year Reanalysis	Ebita et al. (2011)

In the context of this thesis it is worth commenting that precipitation is not assimilated in any of the products listed in Table 3.1, instead it is fully model generated. However, meteorological variables that affect precipitation are still assimilated.

3.2 Climate model output

Similar to reanalysis products, climate models provide gridded datasets of climate related variables. However, how this data is generated is very different. Whereas weather models aim for short integration times with a frequent input of observations, climate models aim for long integration times with no continuous input of observations. In some instances climate models use starting conditions based on observations. Here it is also important to note the differences between fully coupled climate models and non/sparsely coupled climate models. A *coupled* climate model is used to fully simulate the climate system. It consists of multiple *coupled* models, each responsible for its own domain, e.g.: atmosphere, ocean, vegetation, and sea ice. The coupled models communicate with each other, so that for instance the ocean can influence the atmosphere which in turn can affect the ocean. This enables the model to run freely for long time periods without additional input, since the different models update the model state continuously. Non or sparsely coupled climate models replace some, or all but one, of the domain-specific models with pre-computed datasets of key variables. Consequently, the pre-computed variable(s) will not respond to the coupled model(s). Because of the added complexity and long

integration times of climate models they are usually run at a coarser spatial resolution compared to reanalysis products to make them computationally feasible. At these resolutions, climate models cannot physically represent all processes in the climate systems, as some processes occur at scales lower than the spatial and temporal resolution of the model. Instead, the models use simplified, or parametrized, implementations of these processes. Both weather and climate models use parameterizations, but climate models often parametrize more processes and use simpler parameterizations. Parameterizations are typically based on observed empirical relationships, which allow the model to bypass the physical relationship — lowering the computational requirements. Across different climate models, not only do the implementations of these parameterizations differ, but there is also a large variety in e.g. how the spatial grid is represented, how the dynamics are solved, and how domain-models are coupled. As a consequence, there is a great diversity in climate models, all representing the climate slightly different from the other.

The goal of the initial Coupled Model Intercomparison Project (CMIP) from the World Climate Research Programme (WCRP), and subsequent phases, is to make use of these model variations to quantify the uncertainties, but also importantly the consistencies, across the output of different climate models — to improve the understanding of the climate of the past, present, and future. This is achieved by designing standardized experiments that provide common boundary conditions and simulation protocols for the models, which are run by the participating modelling groups. Examples of these experiments include:

- A historical control run where boundary conditions such as GHG concentrations, land use, and solar forcing are based on historical (1850–2014) observations.

- An abrupt 4x increase in CO_2 concentrations compared to historical values, after which the model runs free with constant CO_2 concentrations for at least 150 years.

- Future projections of the 21st century and beyond, based on Shared Socioeconomic Pathways (SSPs) and Representative Concentration Pathways (RCPs). The SSPs and RCPs are used to create scenarios of e.g. future emissions and land use changes, which in turn acts as boundary conditions for the models.

Since its inception, the experiments run under the CMIP umbrella have increased: under the sixth phase, CMIP6, there are 21 different MIPs endorsed by CMIP. The experiments include a wide range of topics: from sea ice, aerosols, clouds, and geoengineering, to scenarios of the future (Eyring et al., 2016). Since one of the main goals of CMIP is to characterize model differences, a large part of the project is also about archiving the data produced through the experiments and making it available to researchers. This allows more groups to analyse the data, and to create additional MIPs not officially endorsed by CMIP. One of the projects that make use of CMIP-data is ARTMIP (see Section 3.4).

3.3 Detecting and tracking atmospheric rivers

ARs are detected using satellite observations (e.g. Ralph et al., 2004), or, more commonly today using gridded datasets such as reanalysis products or the output from weather or climate models (e.g. Guan & Waliser, 2015). Satellite observations generally consists of the Integrated Water Vapour (IWV) while approaches using reanalysis or model data use either IWV or the Integrated water Vapour Transport (IVT). The IWV ($\mathrm{kg\,m^{-2}}$) describes the total moisture content integrated over the atmospheric column from the surface (p_{sfc}) to e.g. 200 hPa:

$$\mathrm{IWV} = -\frac{1}{g}\int_{p_{\mathrm{sfc}}}^{200} q(p)dp, \tag{3.1}$$

where g is the gravitational acceleration ($\mathrm{m\,s^{-2}}$) and q is the specific humidity ($\mathrm{kg\,kg^{-1}}$) at pressure level p (hPa). The IVT ($\mathrm{kg\,m^{-1}\,s^{-1}}$) combines the IWV with the horizontal wind components u and v ($\mathrm{m\,s^{-1}}$) to describe the moisture transport integrated over the atmospheric column:

$$\mathrm{IVT} = \frac{1}{g}\sqrt{\left(\int_{p_{\mathrm{sfc}}}^{200} q(p)u(p)\,dp\right)^2 + \left(\int_{p_{\mathrm{sfc}}}^{200} q(p)v(p)\,dp\right)^2}. \tag{3.2}$$

Regardless of the data used, methods employed to detect ARs apply some type of criteria to the IWV or IVT field to detect regions with high moisture content or transport. Typically, this involves first applying a threshold to the field to remove the background moisture. This results in multiple separate contiguous regions of high moisture. These regions are the initial AR candidates. However, a region with an unusually high moisture content is not automatically an AR, as there are many processes that lead to elevated levels of moisture. The remote transport of moisture in ARs is only one of them. Because of this, the initial AR regions are further filtered via for instance geometric constraints to identify the actual ARs. The general steps of an ARDT are shown in Fig. 3.1.

3.3.1 AR detection algorithms

The criteria used in AR identification differ substantially among the Atmospheric River Detection and Tracking algorithms (ARDTs) published in the scientific literature. The approaches using the IWV often use a threshold of 2 cm (e.g. Dettinger et al., 2011; Goldenson et al., 2018; Ralph et al., 2004), and can be combined with thresholds on other variables such as wind speed (e.g. Hagos et al., 2015). The AR candidates are then filtered by length (> 2000 km) and width (< 1000 km) to identify the long and narrow regions of high moisture, characteristic for ARs.

The ARDTs using IVT show a large variety for both the initial threshold and geometric filters. These ARDTs can be grouped by if the initial IVT-threshold is fixed or variable in some way. The fixed threshold ARDTs apply a constant value to all grid points, e.g. $\mathrm{IVT} \geq 500\,\mathrm{kg\,m^{-1}\,s^{-1}}$ (Reid et al., 2020). The variable threshold ARDTs on the other hand employ a threshold that vary

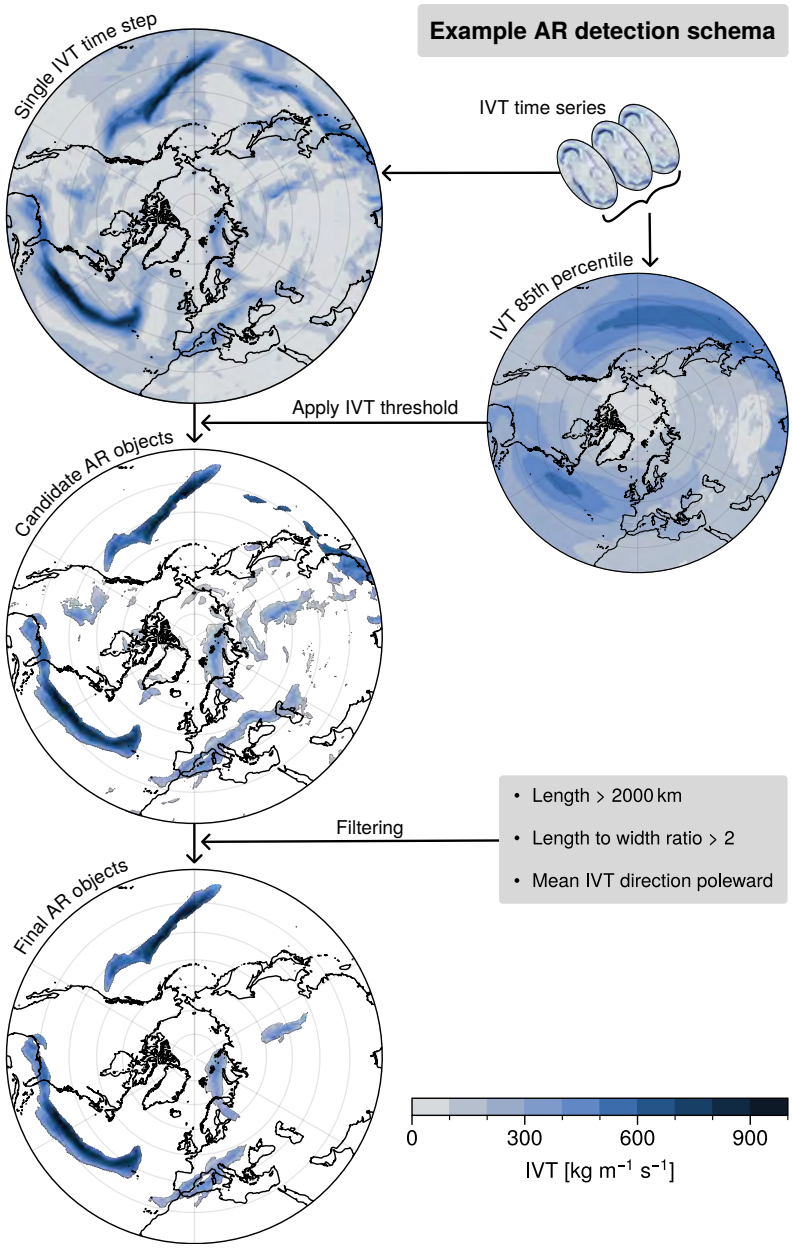

Figure 3.1: Example schema of an AR detection algorithm, based on the GuanWaliser_v2 ARDT. First, the IVT time series is used to calculate the 85th percentile IVT over time. Second, the percentile is applied as a threshold to each time step. Third, the resulting AR candidates are filtered by length, length to width ratio, and the mean IVT direction.

spatially, and sometimes with time. The spatial variation is achieved by for instance using the 85th percentile of the IVT climatology (e.g. Guan & Waliser, 2015; Lavers et al., 2015). Similar to the IWV-based methods, and regardless of the type of threshold, the resulting contiguous areas are filtered by length, width, and often by other attributes, such as IVT direction (Guan & Waliser, 2015; Leung & Qian, 2009) and latitudinal movement (Ramos et al., 2016). The IVT direction and movement of the AR candidates are examined to make sure the moisture transport has a strong meridional component, as this is part of some AR definitions. The direction can also be used to differentiate the ARs from the high moisture within an extratropical cyclone. Additionally, some ARDTs require the ARs to extend over multiple time steps. This adds the additional step of tracking the separate ARs through time.

In my research I have used the results from four different ARDTs: GuanWaliser_v2, Mundhenk_v3, Reid500, and TempestLR. These ARDTs are described in detail below. Fig. 3.2 shows how the extent and number of ARs in a single time step vary among these four ARDTs.

GuanWaliser_v2 (Guan & Waliser, 2015, 2019)

The GuanWaliser_v2 ARDT uses a variable IVT-threshold. The IVT-threshold is based on the climatological and season-dependent 85th percentile. This enables the threshold to vary in both space and by season. Simultaneously, IVT is not allowed to be below $100\,\mathrm{kg\,m^{-1}\,s^{-1}}$. The resulting objects (areas of connected pixels) are then filtered using the following conditions:

- Mean direction of IVT over the object should be $> 50\,\mathrm{kg\,m^{-1}\,s^{-1}}$ poleward.
- AR length $> 2000\,\mathrm{km}$
- AR length to width ratio > 2

Here it is worth noting that the method used to find the main axes, and thus lengths, of the ARs inherently makes sure that ARs that pass the length-to-width ratio criteria also have a coherent IVT direction. Furthermore, AR candidates with circular axes are typically embedded in tropical cyclones and are filtered out. For any AR objects filtered out by the above criteria, the initial percentile threshold is increased by 2.5 percentiles and the object is sent through another iteration of the algorithm. This continues iteratively until the 95th percentile. Iteratively raising the threshold percentile extracts possible ARs from larger areas with high moisture levels. At this point, all AR objects that have been filtered out are discarded.

Mundhenk_v3 (Mundhenk et al., 2016)

The Mundhenk_v3 ARDT applies a static IVT-threshold of $250\,\mathrm{kg\,m^{-1}\,s^{-1}}$ to a field of IVT anomalies. The anomalous IVT field is generated by removing the mean and the seasonal cycle of the time series in each grid point. This removes the slow evolving features of the IVT. Despite using a static threshold,

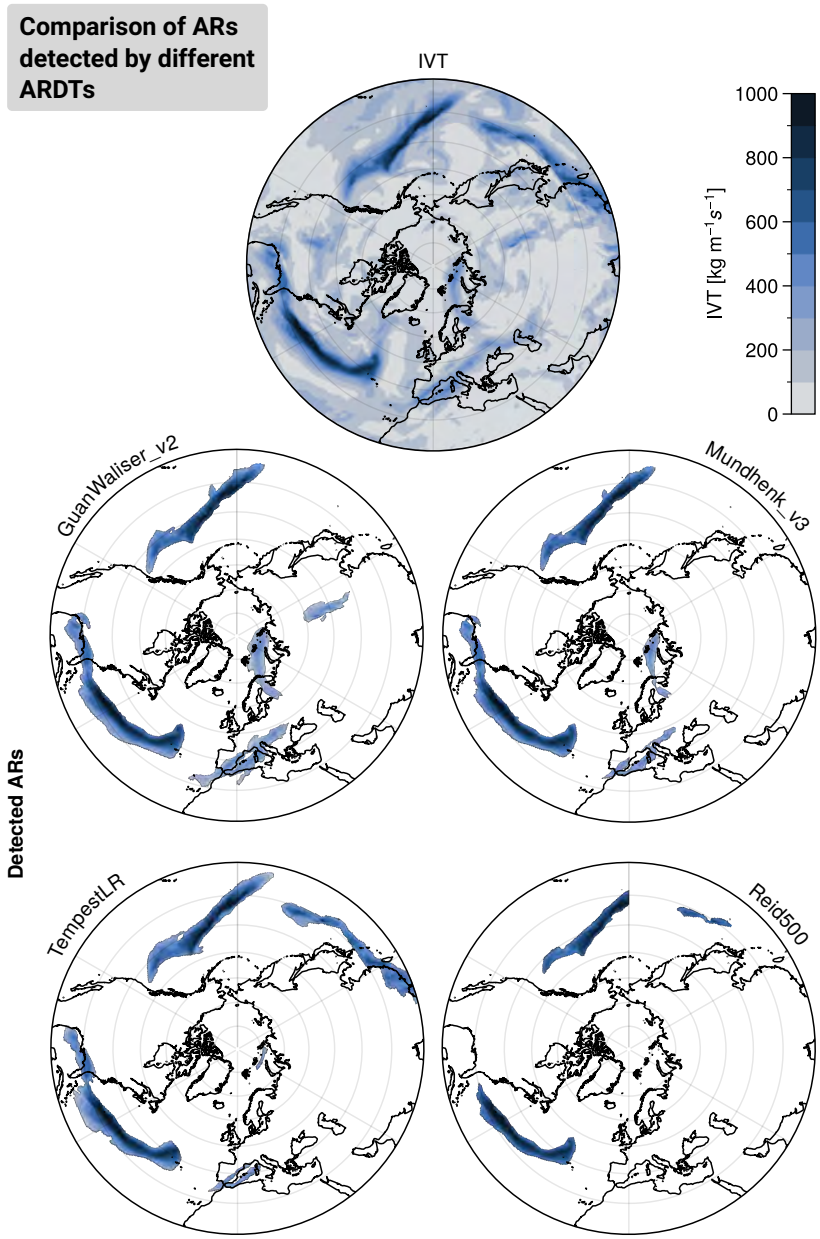

Figure 3.2: Comparison of ARs detected by four different ARDTs for a single time step. The top centre panel shows the IVT during the time step, and the four lower panels show the ARs detected by the GuanWaliser_v2, Mundhenk_v3, TempestLR, and Reid500 ARDTs.

the use of IVT anomalies enable the threshold to behave as if it varied in both space and time. The resulting AR objects are subsequently filtered for:

- The contiguous object should consist of at least 150 grid points
- Major axis length ≥ 25 grid points
- Width to length ratio ≥ 1.6
- Mean anomalous IVT $\geq 305\,\mathrm{kg\,m^{-1}\,s^{-1}}$
- Orientation from parallels > 0.95 radians, latitude of centre of mass $> 20°$N

Circular objects are removed by evaluating the eccentricity of an ellipsis with the same second moments as the candidate AR object. Additionally, AR objects that pass the filtering described above but contain multiple anomalous IVT peaks are further segmented and subsequently filtered again.

Reid500 (Reid et al., 2020)

The Reid500 ARDT applies a fixed threshold of $500\,\mathrm{kg\,m^{-1}\,s^{-1}}$ to the IVT field to extract the candidate AR objects. It then fits an ellipsoid to each of the extracted AR objects. The ellipsoid is used compute the following AR parameters: mean IVT, maximum IVT, major axis length, minor axis length, and orientation. These parameters are used to filter the candidate objects:

- Major axis length $> 2000\,\mathrm{km}$
- Length to width ratio > 2
- Orientation angle must exceed 10° relative to lines of latitude. This removes zonally oriented structures

Any object that does not fulfil all the criteria above is discarded. The Reid family of ARDTs has been tested with different values for the initial IVT-threshold, from 150 to $1000\,\mathrm{kg\,m^{-1}\,s^{-1}}$. However, not all of these AR catalogues are published through ARTMIP.

TempestLR (McClenny et al., 2020; Rhoades et al., 2020; Ullrich & Zarzycki, 2017)

While the TempestLR ARDT still uses the IVT, it takes a slightly different approach and analyses individual grid points for AR conditions using the Laplacian of the IVT field. In this context, the Laplacian operator will highlight regions of strong curvature in IVT — which could correspond to ARs, due to their ridge-like nature. The algorithm, which is applied to each grid point, is described below:

- The grid point should be poleward of 20° N/S
- The Laplacian of the IVT field, which is computed using a stencil radius of 800 km and 9 discrete points, should be $< -40\,000\,\mathrm{kg\,m^{-1}\,s^{-1}\,rad^{-2}}$.

- The grid point should be part of a group of at least 50 connected grid points that meet the above criteria. This corresponds to an area of approximately 125 000 km^2 at a 0.5° horizontal resolution. The group is computed using a flood fill algorithm.
- The grid point is not part of a tropical cyclone. The points within a tropical cyclone are filtered using a separate detection algorithm designed for tropical cyclones part of the same software package as the TempestLR ARDT. It masks all grid points within an 8° radius of grid points that meet the following conditions:
  - Is the most intense local minimum sea-level-pressure within 2.0°.
  - Sea-level pressure increase at least 375 Pa over a 3.6° radius.
  - The thickness of the 300–500 hPa geopotential height should decrease by 6 meters over 7.5°.

In practice, the fixed threshold applied to the Laplacian IVT in TempestLR ARDT lets the algorithm work similarly to a variable threshold ARDT, as it detects rapid changes, or ridges, in the IVT field regardless of the background climatology. Furthermore, trials have shown that the TempestLR does not flag any points with IVT $\leq 250\,kg\,m^{-1}\,s^{-1}$ as ARs.

3.4 An overview of the Atmospheric River Tracking Method Intercomparison Project

The goal of the Atmospheric River Tracking Method Intercomparison Project (ARTMIP; Shields et al., 2018) is to explore how technical and conceptual differences among ARDTs affect the perceived role of ARs in the climate system. As an intercomparison project, it defines a set of experiments for the participating ARDTs to run. The ARs identified in the different experiments are collected in so called AR catalogues, one for each ARDT and experiment. ARTMIP also coordinates the initial analysis of these AR catalogues, and makes them publically available in a central repository. The ARTMIP experiments are grouped into two tiers:

Tier 1

The goal of tier 1 is to establish baseline AR detection statistics for all participating ARDTs. For this purpose, research groups run their ARDTs on data from the MERRA-2 reanalysis product. The dataset covers the period from January 1980 to June 2017 at a 3-hourly resolution, and has a horizontal resolution of $0.625° \times 0.5°$ (Shields et al., 2018).

A total of 22 ARDTs participated in the tier 1 experiment, and the results are presented and analysed in Rutz et al. (2019). In the study, AR catalogues were evaluated along three transects: the North American West Coast, the interior of western North America, and the European West Coast. The analysis shows that AR frequencies vary greatly depending on the ARDT, with slightly

higher ARDT differences for the two more coastal transects. Furthermore, ARDTs employing an absolute threshold show stronger latitudinal frequency variations compared to the relative threshold ARDTs. At the slightly higher latitudes of Western Europe, the absolute threshold ARDTs show overall higher AR frequencies compared to N. America. This is thought to be attributable to the climatologically higher IVT at these latitudes. Similarly, AR duration varies depending on the ARDT, although not to the same extent as AR frequency. The duration appears dependent on a relationship between latitude and the type of IVT-threshold — relative threshold ARDTs results in longer AR durations at lower latitudes.

Overall, the tier 1 experiment shows that ARDT differences give rise to a large degree of uncertainty in the climatological characteristics of ARs. These uncertainties can be reduced by grouping the ARDTs based on the type of threshold they use, however, even within these groups uncertainties remain due to differences in for instance threshold magnitude and geometric filtering.

Tier 2

Tier 2, described in Shields et al. (2018), is similar in setup to tier 1. The different working groups use their ARDTs to produce AR catalogues based on predefined datasets of atmospheric moisture transport. However, tier 2 could be considered more as a group of sub-experiments, all of which aim to explore how sensitive the resulting AR climatologies are to differences in the input data. There are three sub-experiments in tier 2:

High-resolution climate change experiment

This experiment aims to evaluate how climate model resolution affects simulated AR characteristics. The ARDTs are run on datasets that was generated using the Community Atmosphere Model, version 5 (CAM5). The first dataset consists of 27 years for data (1979–2005) representing the recent past, available at three different horizontal resolutions: 25, 100, and 200 km. The second dataset covers the end of the century (2079–2099) under the RCP8.5 scenario, at a 25 km resolution (Shields et al., 2018). The tier 2 high resolution experiment does not analyse longer, transient, climate projections. Instead, it focuses on the representation of regional details, and how AR characteristics of the climate model runs compares to results from tier 1 (Shields et al., 2023).

The results of the tier 2 high resolution experiment is presented in Shields et al. (2023). 14 different ARDTs contributed to this sub-experiment, all of which also contributed to tier 1. AR catalogues of the modelled recent past agrees well with results from the reanalysis based tier 1 over the main global AR areas, with relatively high agreement among ARDTs. There is also consensus among the ARDTs in how much global AR frequencies will change by the end of the century. Regionally the uncertainty increases, with AR occurrence showing a large spread during all months across the ARDTs. However, the seasonal cycle in MERRA-2 is fairly well represented in both the modelled recent past and end of the century. Generally, the spread is lower among the less restrictive

relative threshold ARDT. Simultaneously, the intensity of AR-related regional precipitation is shown to increase, with rain rates of 50–200 mm/day becoming more common. These results highlight the value of employing both relative and absolute threshold ARDTs when investigating how ARs, and their impacts, will change with the changing climate.

CMIP5 and CMIP6 experiments

For this group of experiments, initially described in Shields et al. (2018) and in further detail in O'Brien et al. (2022), research groups run ARDTs on output from climate models part of CMIP5 (e.g. Taylor et al., 2012) and CMIP6 (e.g. Eyring et al., 2016). Specifically, they use model output from the historical simulations and from model runs based on the RCP8.5 (CMIP5) and SSP5-8.5 (CMIP6) scenarios. In addition to investigating possible trends in AR frequency, the multi-model and multi-ARDT approach lets researchers compare the magnitudes of ARDT and model associated uncertainty.

The working groups of tier 2 CMIP5 and CMIP6 used 9 different climate models from CMIP5 (n=6) and CMIP6 (n=3) together with 6 different ARDTs in their assessment, which is presented in O'Brien et al. (2022). All outputs use a 6-hourly resolution and were regridded to a common $4^\circ \times 5^\circ$ latitude-longitude grid. They found very good agreement between the AR frequency patterns of the modelled historical climate and those from MERRA-2 (form Tier 1). Since the distinctive spatial patterns of each ARDT is present in both simulations and the reanalysis, they determine that AR characteristics appear to not be sensitive to how atmospheric dynamics are represented in the models. However, the magnitude of the projected changes in AR frequency vary substantially among the ARDT and model combinations, with average increases ranging between 20–30 %. It is also important to note that ARs will become more common in areas with previously low AR frequencies, such as Southern Africa and the Arctic Ocean. The differences among ARDTs are largely attributed to whether the ARDT is using a fixed or variable IVT-threshold: ARDTs that use a threshold that is fixed in time give higher future AR frequencies, whereas ARDTs that use a threshold varying in time show smaller changes in the future. Instead, these ARDTs show, to a larger degree, a future poleward shift of ARs. Furthermore, fixed threshold ARDTs appear to be more sensitive to the thermodynamical changes of the climate, while variable threshold ARDTs appear more sensitive to dynamical changes of the climate. Because of these differences, the authors conclude that new projects investigating AR statistics should design their experiments to include ARDT uncertainty.

Reanalysis experiments

The tier 2 reanalysis experiment is essentially an expansion of tier 1, extending it with additional reanalysis products. The setup of the experiment, and the results, are presented in Collow et al. (2022). They analysed 11 different ARDTs, applied to three different reanalysis products covering the period 1980–2019: MERRA-2 (1-hourly), ERA5 (1-hourly), and JRA-55 (6-hourly). The reanalysis products were used at their native horizontal resolution. Seven of the

ARDTs participating in the study were applied globally, while the remaining four are designed for specific regions.

As background to the subsequent AR analysis, Collow et al. (2022) presents a comparison of key AR-related variables between the three reanalysis products. For global means, MERRA-2 exhibits overall higher water vapour content and IVT compared to both ERA5 and JRA-55. Contrastingly, JRA-55 shows slightly higher global mean precipitation compared to ERA5 and MERRA-2. However, despite the differences in magnitude, the global means of IWV, IVT, and precipitation for all three products are well correlated through time.

Comparable to the results of tier 1, the global ARDTs in tier 2 detect similar spatial AR frequency patterns across the three reanalysis products. Yet, because of the underlying differences in IVT, the magnitude of AR frequencies varies across the reanalysis products. Comparing MERRA-2 and ERA5, more ARs are found in MERRA-2 because of the overall higher IVT. These differences are to some extent reduced between ARDTs that employ a variable IVT-threshold. These types of ARDTs could be thought of as retuning themselves to the background climate, since the threshold is based on the climatology of the input data. Because of this, the authors suggest that fixed IVT-threshold ARDTs should be retuned depending on the input data, to better reflect what constitutes AR conditions in the specific dataset.

Overall, the AR characteristics of MERRA-2 and JRA-55 show strong agreement. However, AR frequencies are lower for a few of the fixed threshold ARDTs. They attribute this to the coarser resolution of JRA-55 in two different ways: First, the coarser resolution limits the capability of the reanalysis to represent very high IVT: this impacts ARDTs using particularly high IVT-thresholds. Second, the coarser resolution results in overall weaker IVT gradients: this affects the TempestLR ARDT in particular. The increased horizontal resolution of ERA5 improves the representation of regional features such as coastlines and topography, which consequently leads to higher detail in the AR characteristics for all ARDTs. The different resolutions of the reanalysis products also influence the AR associated precipitation, as this is mostly driven by topography. Despite this, the spatial patterns of AR associated precipitation are relatively similar between the reanalysis products, but with an apparent loss of detail with decreasing resolution.

The key takeaway from the tier 2 reanalysis experiment is that differences in AR characteristics due to ARDT is larger than differences due to reanalysis products. Similar to findings from other ARTMIP experiments, this highlights the value of using multiple ARDTs in AR analysis. The authors also note that combining regional and global ARDTs should be avoided, as these ARDTs are designed for different scientific questions and are therefore not directly comparable. Additionally, high resolution reanalysis products are preferred for regional AR analysis.

Chapter 4

Summary of included papers and future work

4.1 Paper 1: A climatology of atmospheric rivers over Scandinavia and associated precipitation

Previous AR research has mostly had a global focus, investigating large scale patterns and assessing the overall AR characteristics over continents such as Asia, Europe, and North America (see Section 2.1). While more regional AR studies that present detailed AR climatologies exist, a majority of these concern the west coast of North America. The few studies on ARs over Scandinavia are investigating more specific case studies, and provide valuable information for the events in question, but are too limited in both space and time to be generalizable over the region. There was no detailed climatology of ARs over Scandinavia prior to this study.

Therefore, with this paper we establish a detailed climatology of the ARs that make landfall over Scandinavia, and how they are related to the regional precipitation. We used four different AR catalogues, part of ARTMIP, that are all based on 40 years (1980–2019) of ERA5 reanalysis data. The ARDT-ensemble enabled us to examine the consistency of our results across the different implementations of ARDTs. Overall, we found that ARs over Scandinavia are most active over Denmark and southern Norway, where the annual average AR frequencies reach up to 5.9 %. At the same time, some locations in Scandinavia, notably western Norway, receive up 40.7 % of its annual precipitation during AR events.

To identify common AR pathways and further explain how ARs influence weather and climate over Scandinavia, we clustered the individual ARs using the K-means algorithm. We found four main AR pathways where ARs make landfall over Scandinavia (maximum annual AR frequencies and AR-related precipitation in parentheses): over southern Denmark (4.2 %, 19.7 %), along

the northern coast of Norway (2.6 %, 13.1 %), over southern parts of Norway and south-central parts of Sweden (2.0 %, 15.1 %), and along the southern coast of Norway (1.1 %, 7.8 %). Further analysis showed that the ARs over Scandinavia are the least common during spring and most frequent in autumn. However, the seasonality varies between the different AR pathways. Grouping ARs according to the phase of the NAO showed that ARs over Scandinavia are affected by the large scale circulation: Scandinavian ARs are generally more frequent during strong positive phases (> 1.5) of the NAO. However, here there are some notable differences among the AR pathways. The frequency of the more northern ARs increase almost linearly with the increasing phase of the NAO. This differs from the southernmost ARs, which appear less linearly correlated with the phase of the NAO: frequencies reach a minimum during neutral phases of the NAO and increase during negative and positive phases alike.

With this study, we have established a detailed AR climatology over Scandinavia, which serves as a good foundation for future AR-related studies over the region. Future research could continue to explore the current AR–weather relationships, or use this climatology as a basis for studies that investigate changes to ARs during the 21st century. To my knowledge, identifying AR pathways by clustering is novel to this paper, and the method can relatively easily be applied to other regions, whether these be countries, river basins, or ice sheets.

4.2 Future work

Now that we have established a climatology of ARs over Scandinavia, a simple follow-up question is how AR frequencies will change during the 21st century. There are currently a collection of published studies that have investigated AR characteristics during the 21st century using climate projections. However, these studies generally have a global context, analysing large-scale patterns. For a more regional analysis over Scandinavia, additional research is still possible. To this end, the methods of Paper I can be adapted and applied to compatible AR catalogues from the tier 2 CMIP5 and CMIP6 experiment of ARTMIP. The model-generated AR catalogues from this experiment cover the climate of the recent past and the 21st century under the RCP8.5 and SSP5-8.5 scenarios. The resulting AR frequencies, based on the modelled climate, can then be assessed for potential trends and shifts in location of AR patterns. Importantly, the baseline from Paper I can be used to evaluate potential biases in the climate models. Furthermore, the use of clustered AR pathways, introduced in Paper I, provide an increased level of detail to the evaluation of the response of ARs to climate change. Potentially, this could highlight how different ARs respond differently to the changing climate, and what the drivers behind this varying response is.

There is still potential for interesting work on how ARs affect the surface energy balance in the climatologically dry high latitude regions. Here, previous research has focused on how ARs affect for instance the recovery of sea ice in the Arctic, or the mass balance of the Greenland ice sheet. However, outside of Greenland, Antarctica, and a few river basins, less work has been done to understand the relationship between ARs, snowfall and variations in the snow cover. Here, the moisture transported through ARs can:

- precipitate as snow and contribute to the snow cover,
- precipitate as rain and contribute to melting the snow cover,
- increase temperatures and contribute to melting the snow cover.

These processes present a possible mechanism for how ARs could influence the surface albedo at larger scales. A link between ARs and the surface albedo would be exciting, as it opens up further avenues for how ARs could play a role in Arctic amplification.

Bibliography

Azad, R., & Sorteberg, A. (2017). Extreme daily precipitation in coastal western Norway and the link to atmospheric rivers. *Journal of Geophysical Research: Atmospheres*, *122*(4), 2080–2095. https://doi.org/10.1002/2016JD025615 (cit. on p. 13).

Bao, J.-W., Michelson, S. A., Neiman, P. J., Ralph, F. M., & Wilczak, J. M. (2006). Interpretation of Enhanced Integrated Water Vapor Bands Associated with Extratropical Cyclones: Their Formation and Connection to Tropical Moisture. *Monthly Weather Review*, *134*(4), 1063–1080. https://doi.org/10.1175/MWR3123.1 (cit. on p. 5).

Benedict, I., Ødemark, K., Nipen, T., & Moore, R. (2019). Large-Scale Flow Patterns Associated with Extreme Precipitation and Atmospheric Rivers over Norway. *Monthly Weather Review*, *147*(4), 1415–1428. https://doi.org/10.1175/MWR-D-18-0362.1 (cit. on p. 13).

Blamey, R. C., Ramos, A. M., Trigo, R. M., Tomé, R., & Reason, C. J. C. (2018). The Influence of Atmospheric Rivers over the South Atlantic on Winter Rainfall in South Africa. *Journal of Hydrometeorology*, *19*(1), 127–142. https://doi.org/10.1175/JHM-D-17-0111.1 (cit. on p. 12).

Browning, K. A. (1990). Organization of Clouds and Precipitation in Extratropical Cyclones. In C. W. Newton & E. O. Holopainen (Eds.), *Extratropical Cyclones* (pp. 129–153). American Meteorological Society. https://doi.org/10.1007/978-1-944970-33-8_8 (cit. on p. 3).

Collow, A. B. M., Shields, C. A., Guan, B., Kim, S., Lora, J. M., McClenny, E. E., Nardi, K., Payne, A., Reid, K., Shearer, E. J., Tomé, R., Wille, J. D., Ramos, A. M., Gorodetskaya, I. V., Leung, L. R., O'Brien, T. A., Ralph, F. M., Rutz, J., Ullrich, P. A., & Wehner, M. (2022). An Overview of ARTMIP's Tier 2 Reanalysis Intercomparison: Uncertainty in the Detection of Atmospheric Rivers and Their Associated Precipitation. *Journal of Geophysical Research: Atmospheres*, *127*(8), e2021JD036155. https://doi.org/10.1029/2021JD036155 (cit. on pp. 25, 26).

Dacre, H. F., Clark, P. A., Martinez-Alvarado, O., Stringer, M. A., & Lavers, D. A. (2015). How Do Atmospheric Rivers Form? *Bulletin of the American Meteorological Society*, *96*(8), 1243–1255. https://doi.org/10.1175/BAMS-D-14-00031.1 (cit. on p. 5).

Dacre, H. (2020). A review of extratropical cyclones: Observations and conceptual models over the past 100 years. *Weather*, *75*(1), 4–7. https://doi.org/10.1002/wea.3653 (cit. on p. 4).

Dee, D. P., Uppala, S. M., Simmons, A. J., Berrisford, P., Poli, P., Kobayashi, S., Andrae, U., Balmaseda, M. A., Balsamo, G., Bauer, P., Bechtold, P., Beljaars, A. C. M., van de Berg, L., Bidlot, J., Bormann, N., Delsol, C., Dragani, R., Fuentes, M., Geer, A. J., ... Vitart, F. (2011). The ERA-Interim reanalysis: Configuration and performance of the data assimilation system. *Quarterly Journal of the Royal Meteorological Society*, *137*(656), 553–597. https://doi.org/10.1002/qj.828 (cit. on p. 16).

Dettinger, M. D. (2013). Atmospheric Rivers as Drought Busters on the U.S. West Coast. *Journal of Hydrometeorology*, *14*(6), 1721–1732. https://doi.org/10.1175/JHM-D-13-02.1 (cit. on p. 11).

Dettinger, M. D., Ralph, F. M., Das, T., Neiman, P. J., & Cayan, D. R. (2011). Atmospheric Rivers, Floods and the Water Resources of California. *Water*, *3*(2), 445–478. https://doi.org/10.3390/w3020445 (cit. on pp. 11, 18).

Ebita, A., Kobayashi, S., Ota, Y., Moriya, M., Kumabe, R., Onogi, K., Harada, Y., Yasui, S., Miyaoka, K., Takahashi, K., Kamahori, H., Kobayashi, C., Endo, H., Soma, M., Oikawa, Y., & Ishimizu, T. (2011). The Japanese 55-year Reanalysis "JRA-55": An Interim Report. *Sola*, *7*, 149–152. https://doi.org/10.2151/sola.2011-038 (cit. on p. 16).

Eiras-Barca, J., Lorenzo, N., Taboada, J., Robles, A., & Miguez-Macho, G. (2018). On the relationship between atmospheric rivers, weather types and floods in Galicia (NW Spain). *Natural Hazards and Earth System Sciences*, *18*(6), 1633–1645. https://doi.org/10.5194/nhess-18-1633-2018 (cit. on p. 12).

Eyring, V., Bony, S., Meehl, G. A., Senior, C. A., Stevens, B., Stouffer, R. J., & Taylor, K. E. (2016). Overview of the Coupled Model Intercomparison Project Phase 6 (CMIP6) experimental design and organization. *Geoscientific Model Development*, *9*(5), 1937–1958. Retrieved September 27, 2023, from https://gmd.copernicus.org/articles/9/1937/2016/ (cit. on pp. 17, 25).

Gelaro, R., McCarty, W., Suárez, M. J., Todling, R., Molod, A., Takacs, L., Randles, C. A., Darmenov, A., Bosilovich, M. G., Reichle, R., Wargan, K., Coy, L., Cullather, R., Draper, C., Akella, S., Buchard, V., Conaty, A., Silva, A. M. da, Gu, W., ... Zhao, B. (2017). The Modern-Era Retrospective Analysis for Research and Applications, Version 2 (MERRA-2). *Journal of Climate*, *30*(14), 5419–5454. https://doi.org/10.1175/JCLI-D-16-0758.1 (cit. on p. 16).

Gimeno, L., Nieto, R., Vázquez, M., & Lavers, D. A. (2014). Atmospheric rivers: A mini-review. *Frontiers in Earth Science*, *2*. https://doi.org/10.3389/feart.2014.00002 (cit. on pp. 3, 7).

Goldenson, N., Leung, L. R., Bitz, C. M., & Blanchard-Wrigglesworth, E. (2018). Influence of Atmospheric Rivers on Mountain Snowpack in the Western United States. *Journal of Climate*, *31*(24), 9921–9940. https://doi.org/10.1175/JCLI-D-18-0268.1 (cit. on p. 18).

Gorodetskaya, I. V., Durán-Alarcón, C., González-Herrero, S., Clem, K. R., Zou, X., Rowe, P., Rodriguez Imazio, P., Campos, D., Leroy-Dos Santos, C.,

Dutrievoz, N., Wille, J. D., Chyhareva, A., Favier, V., Blanchet, J., Pohl, B., Cordero, R. R., Park, S.-J., Colwell, S., Lazzara, M. A., … Picard, G. (2023). Record-high Antarctic Peninsula temperatures and surface melt in February 2022: A compound event with an intense atmospheric river. *npj Climate and Atmospheric Science*, *6*(1), 1–18. https://doi.org/10.1038/s41612-023-00529-6 (cit. on p. 12).

Guan, B., & Waliser, D. E. (2015). Detection of atmospheric rivers: Evaluation and application of an algorithm for global studies: Detection of Atmospheric Rivers. *Journal of Geophysical Research: Atmospheres*, *120*(24), 12514–12535. https://doi.org/10.1002/2015JD024257 (cit. on pp. 6, 7, 11, 18, 20).

Guan, B., & Waliser, D. E. (2019). Tracking Atmospheric Rivers Globally: Spatial Distributions and Temporal Evolution of Life Cycle Characteristics. *Journal of Geophysical Research: Atmospheres*, *124*(23), 12523–12552. https://doi.org/10.1029/2019JD031205 (cit. on pp. 11, 12, 20).

Hagos, S., Leung, L. R., Yang, Q., Zhao, C., & Lu, J. (2015). Resolution and Dynamical Core Dependence of Atmospheric River Frequency in Global Model Simulations. *Journal of Climate*, *28*(7), 2764–2776. https://doi.org/10.1175/JCLI-D-14-00567.1 (cit. on p. 18).

Hersbach, H., Bell, B., Berrisford, P., Hirahara, S., Horányi, A., Muñoz-Sabater, J., Nicolas, J., Peubey, C., Radu, R., Schepers, D., Simmons, A., Soci, C., Abdalla, S., Abellan, X., Balsamo, G., Bechtold, P., Biavati, G., Bidlot, J., Bonavita, M., … Thépaut, J.-N. (2020). The ERA5 global reanalysis. *Quarterly Journal of the Royal Meteorological Society*, *146*(730), 1999–2049. https://doi.org/10.1002/qj.3803 (cit. on p. 16).

Hurrell, J. W. (1995). Decadal Trends in the North Atlantic Oscillation: Regional Temperatures and Precipitation. *Science*, *269*(5224), 676–679. https://doi.org/10.1126/science.269.5224.676 (cit. on p. 6).

Hurrell, J. W., & Deser, C. (2010). North Atlantic climate variability: The role of the North Atlantic Oscillation. *Journal of Marine Systems*, *79*(3), 231–244. https://doi.org/10.1016/j.jmarsys.2009.11.002 (cit. on p. 6).

Hurrell, J. W., Kushnir, Y., Ottersen, G., & Visbeck, M. (2003). An Overview of the North Atlantic Oscillation. In *The North Atlantic Oscillation: Climatic Significance and Environmental Impact* (pp. 1–35). American Geophysical Union (AGU). https://doi.org/10.1029/134GM01 (cit. on p. 6).

Ionita, M., Nagavciuc, V., & Guan, B. (2020). Rivers in the sky, flooding on the ground: The role of atmospheric rivers in inland flooding in central Europe. *Hydrology and Earth System Sciences*, *24*(11), 5125–5147. https://doi.org/10.5194/hess-24-5125-2020 (cit. on p. 12).

IPCC. (2023). Annex IV: Modes of Variability. In *Climate Change 2021 – The Physical Science Basis: Working Group I Contribution to the Sixth Assessment Report of the Intergovernmental Panel on Climate Change* (pp. 2153–2192). Cambridge University Press. https://doi.org/10.1017/9781009157896.018 (cit. on pp. 5, 7, 8).

Kamae, Y., Mei, W., & Xie, S.-P. (2017). Climatological Relationship between Warm Season Atmospheric Rivers and Heavy Rainfall over East Asia.

Journal of the Meteorological Society of Japan. Ser. II, *95*(6), 411–431. https://doi.org/10.2151/jmsj.2017-027 (cit. on p. 11).

Kim, J., Moon, H., Guan, B., Waliser, D. E., Choi, J., Gu, T.-Y., & Byun, Y.-H. (2021). Precipitation characteristics related to atmospheric rivers in East Asia. *Int. J. Climatol*, *41*, E2244–E2257. Retrieved June 23, 2025, from https://www.researchgate.net/profile/Hyejin-Moon-2/publication/345372921_Precipitation_characteristics_related_to_atmospheric_rivers_in_East_Asia/links/63f81801b1704f343f77442c/Precipitation-characteristics-related-to-atmospheric-rivers-in-East-Asia.pdf (cit. on p. 12).

Kingston, Daniel. G., Lavers, D. A., & Hannah, D. M. (2016). Floods in the Southern Alps of New Zealand: The importance of atmospheric rivers. *Hydrological Processes*, *30*(26), 5063–5070. https://doi.org/10.1002/hyp.10982 (cit. on p. 12).

Kump, L. R., Kasting, J. F., & Crane, R. G. (2014). *The earth system* (3. ed., Pearson new internat. ed). Pearson. (Cit. on p. 8). kumpEarthSystem2014a.

Lauer, M., Rinke, A., Gorodetskaya, I., Sprenger, M., Mech, M., & Crewell, S. (2023). Influence of atmospheric rivers and associated weather systems on precipitation in the Arctic. *Atmospheric Chemistry and Physics*, *23*(15), 8705–8726. https://doi.org/10.5194/acp-23-8705-2023 (cit. on p. 13).

Lavers, D. A., Ralph, F. M., Waliser, D. E., Gershunov, A., & Dettinger, M. D. (2015). Climate change intensification of horizontal water vapor transport in CMIP5. *Geophysical Research Letters*, *42*(13), 5617–5625. https://doi.org/10.1002/2015GL064672 (cit. on p. 20).

Lavers, D. A., & Villarini, G. (2013). The nexus between atmospheric rivers and extreme precipitation across Europe. *Geophysical Research Letters*, *40*(12), 3259–3264 (cit. on pp. 6, 12).

Lavers, D. A., & Villarini, G. (2015). The contribution of atmospheric rivers to precipitation in Europe and the United States. *Journal of Hydrology*, *522*, 382–390. https://doi.org/10.1016/j.jhydrol.2014.12.010 (cit. on p. 12).

Lavers, D. A., Villarini, G., Allan, R. P., Wood, E. F., & Wade, A. J. (2012). The detection of atmospheric rivers in atmospheric reanalyses and their links to British winter floods and the large-scale climatic circulation. *Journal of Geophysical Research: Atmospheres*, *117*(D20), 2012JD018027. https://doi.org/10.1029/2012JD018027 (cit. on pp. 6, 12).

LeGrande, A. N., Booth, J. F., Naud, C. M., Ordaz, C., & Crespo, J. A. (2024). Just How River-Like Are Atmospheric Rivers? *Geophysical Research Letters*, *51*(10), e2023GL105828. https://doi.org/10.1029/2023GL105828 (cit. on pp. 4, 5).

Leung, L. R., & Qian, Y. (2009). Atmospheric rivers induced heavy precipitation and flooding in the western U.S. simulated by the WRF regional climate model. *Geophysical Research Letters*, *36*(3), 2008GL036445. https://doi.org/10.1029/2008GL036445 (cit. on p. 20).

Li, L., Cannon, F., Mazloff, M. R., Subramanian, A. C., Wilson, A. M., & Ralph, F. M. (2024). Impact of atmospheric rivers on Arctic sea ice variations. *The Cryosphere*, *18*(1), 121–137. https://doi.org/10.5194/tc-18-121-2024 (cit. on p. 13).

Liang, J., & Yong, Y. (2021). Climatology of atmospheric rivers in the Asian monsoon region. *International Journal of Climatology*, *41*, E801–E818. Retrieved June 23, 2025, from https://www.researchgate.net/profile/Ju-Liang-2/publication/342649383_Climatology_of_atmospheric_rivers_in_the_Asian_monsoon_region/links/5f75f576299bf1b53e041324/Climatology-of-atmospheric-rivers-in-the-Asian-monsoon-region.pdf (cit. on pp. 11, 12).

Liang, J., Yong, Y., & Hawcroft, M. K. (2023). Long-term trends in atmospheric rivers over East Asia. *Climate Dynamics*, *60*(3), 643–666. https://doi.org/10.1007/s00382-022-06339-5 (cit. on p. 11).

Little, K., Kingston, D. G., Cullen, N. J., & Gibson, P. B. (2019). The Role of Atmospheric Rivers for Extreme Ablation and Snowfall Events in the Southern Alps of New Zealand. *Geophysical Research Letters*, *46*(5), 2761–2771. https://doi.org/10.1029/2018GL081669 (cit. on p. 12).

Maclennan, M. L., Lenaerts, J. T. M., Shields, C. A., Hoffman, A. O., Wever, N., Thompson-Munson, M., Winters, A. C., Pettit, E. C., Scambos, T. A., & Wille, J. D. (2023). Climatology and surface impacts of atmospheric rivers on West Antarctica. *The Cryosphere*, *17*(2), 865–881. https://doi.org/10.5194/tc-17-865-2023 (cit. on p. 12).

Mattingly, K. S., Mote, T. L., & Fettweis, X. (2018). Atmospheric River Impacts on Greenland Ice Sheet Surface Mass Balance. *Journal of Geophysical Research: Atmospheres*, *123*(16), 8538–8560. https://doi.org/10.1029/2018JD028714 (cit. on p. 13).

Mattingly, K. S., Turton, J. V., Wille, J. D., Noël, B., Fettweis, X., Rennermalm, Å. K., & Mote, T. L. (2023). Increasing extreme melt in northeast Greenland linked to foehn winds and atmospheric rivers. *Nature Communications*, *14*(1), 1743. https://doi.org/10.1038/s41467-023-37434-8 (cit. on p. 13).

McClenny, E. E., Ullrich, P. A., & Grotjahn, R. (2020). Sensitivity of Atmospheric River Vapor Transport and Precipitation to Uniform Sea Surface Temperature Increases. *Journal of Geophysical Research: Atmospheres*, *125*(21), e2020JD033421. https://doi.org/10.1029/2020JD033421 (cit. on p. 22).

Mundhenk, B. D., Barnes, E. A., & Maloney, E. D. (2016). All-Season Climatology and Variability of Atmospheric River Frequencies over the North Pacific. *Journal of Climate*, *29*(13), 4885–4903. https://doi.org/10.1175/JCLI-D-15-0655.1 (cit. on p. 20).

Nash, D., Waliser, D., Guan, B., Ye, H., & Ralph, F. M. (2018). The Role of Atmospheric Rivers in Extratropical and Polar Hydroclimate. *Journal of Geophysical Research: Atmospheres*, *123*(13), 6804–6821. https://doi.org/10.1029/2017JD028130 (cit. on p. 3).

Neiman, P. J., Ralph, F. M., Wick, G. A., Lundquist, J. D., & Dettinger, M. D. (2008). Meteorological Characteristics and Overland Precipitation Im-

pacts of Atmospheric Rivers Affecting the West Coast of North America Based on Eight Years of SSM/I Satellite Observations. *Journal of Hydrometeorology*, *9*(1), 22–47. https://doi.org/10.1175/2007JHM855.1 (cit. on p. 7).

Newell, R. E., Newell, N. E., Zhu, Y., & Scott, C. (1992). Tropospheric rivers? – A pilot study. *Geophysical Research Letters*, *19*(24), 2401–2404. https://doi.org/10.1029/92GL02916 (cit. on p. 3).

North, G. R., Pyle, J., & Zhang, F. (2015). *Encyclopedia of Atmospheric Sciences, 6 Volume Set (2nd Edition)* (2nd edition). Elsevier. (Cit. on p. 3).

O'Brien, T. A., Wehner, M. F., Payne, A. E., Shields, C. A., Rutz, J. J., Leung, L.-R., Ralph, F. M., Collow, A., Gorodetskaya, I., Guan, B., Lora, J. M., McClenny, E., Nardi, K. M., Ramos, A. M., Tomé, R., Sarangi, C., Shearer, E. J., Ullrich, P. A., Zarzycki, C., ... Zhou, Y. (2022). Increases in Future AR Count and Size: Overview of the ARTMIP Tier 2 CMIP5/6 Experiment. *Journal of Geophysical Research: Atmospheres*, *127*(6), e2021JD036013. https://doi.org/10.1029/2021JD036013 (cit. on p. 25).

Paltan, H., Waliser, D., Lim, W. H., Guan, B., Yamazaki, D., Pant, R., & Dadson, S. (2017). Global Floods and Water Availability Driven by Atmospheric Rivers. *Geophysical Research Letters*, *44*(20), 10, 387–10, 395. https://doi.org/10.1002/2017GL074882 (cit. on p. 8).

Park, C., Son, S.-W., & Kim, H. (2021). Distinct Features of Atmospheric Rivers in the Early Versus Late East Asian Summer Monsoon and Their Impacts on Monsoon Rainfall. *Journal of Geophysical Research: Atmospheres*, *126*(7), e2020JD033537. https://doi.org/10.1029/2020JD033537 (cit. on p. 12).

Pasquier, J. T., Pfahl, S., & Grams, C. M. (2019). Modulation of atmospheric river occurrence and associated precipitation extremes in the North Atlantic region by European weather regimes. *Geophysical Research Letters*, *46*(2), 1014–1023 (cit. on p. 6).

Philander, S. G. H. (1983). El Niño Southern Oscillation phenomena. *Nature*, *302*(5906), 295–301. https://doi.org/10.1038/302295a0 (cit. on p. 7).

Ralph, F. M., Neiman, P. J., Kiladis, G. N., Weickmann, K., & Reynolds, D. W. (2011). A Multiscale Observational Case Study of a Pacific Atmospheric River Exhibiting Tropical—Extratropical Connections and a Mesoscale Frontal Wave. *Monthly Weather Review*, *139*(4), 1169–1189. https://doi.org/10.1175/2010MWR3596.1 (cit. on p. 7).

Ralph, F. M., Neiman, P. J., & Rotunno, R. (2005). Dropsonde Observations in Low-Level Jets over the Northeastern Pacific Ocean from CALJET-1998 and PACJET-2001: Mean Vertical-Profile and Atmospheric-River Characteristics. *Monthly Weather Review*, *133*(4), 889–910. https://doi.org/10.1175/MWR2896.1 (cit. on pp. 4, 7, 11).

Ralph, F. M., Neiman, P. J., & Wick, G. A. (2004). Satellite and CALJET Aircraft Observations of Atmospheric Rivers over the Eastern North Pacific Ocean during the Winter of 1997/98. *Monthly Weather Review*,

132(7), 1721–1745. https://doi.org/10.1175/1520-0493(2004)132⟨1721:SACAOO⟩2.0.CO;2 (cit. on pp. 4, 5, 11, 18).

Ralph, F. M., Neiman, P. J., Wick, G. A., Gutman, S. I., Dettinger, M. D., Cayan, D. R., & White, A. B. (2006). Flooding on California's Russian River: Role of atmospheric rivers. *Geophysical Research Letters*, *33*(13). https://doi.org/10.1029/2006GL026689 (cit. on p. 11).

Ramos, A. M., Nieto, R., Tomé, R., Gimeno, L., Trigo, R. M., Liberato, M. L., & Lavers, D. A. (2016). Atmospheric rivers moisture sources from a Lagrangian perspective. *Earth System Dynamics*, *7*(2), 371–384 (cit. on pp. 5, 20).

Ramos, A. M., Trigo, R. M., Liberato, M. L. R., & Tomé, R. (2015). Daily Precipitation Extreme Events in the Iberian Peninsula and Its Association with Atmospheric Rivers. *Journal of Hydrometeorology*, *16*(2), 579–597. https://doi.org/10.1175/JHM-D-14-0103.1 (cit. on p. 6).

Reid, K. J., King, A. D., Lane, T. P., & Short, E. (2020). The Sensitivity of Atmospheric River Identification to Integrated Water Vapor Transport Threshold, Resolution, and Regridding Method. *Journal of Geophysical Research: Atmospheres*, *125*(20), e2020JD032897. https://doi.org/10.1029/2020JD032897 (cit. on pp. 18, 22).

Rhoades, A. M., Jones, A. D., O'Brien, T. A., O'Brien, J. P., Ullrich, P. A., & Zarzycki, C. M. (2020). Influences of North Pacific Ocean Domain Extent on the Western U.S. Winter Hydroclimatology in Variable-Resolution CESM. *Journal of Geophysical Research: Atmospheres*, *125*(14), e2019JD031977. https://doi.org/10.1029/2019JD031977 (cit. on p. 22).

Rutz, J. J., Shields, C. A., Lora, J. M., Payne, A. E., Guan, B., Ullrich, P., O'Brien, T., Leung, L. R., Ralph, F. M., Wehner, M., Brands, S., Collow, A., Goldenson, N., Gorodetskaya, I., Griffith, H., Kashinath, K., Kawzenuk, B., Krishnan, H., Kurlin, V., … Viale, M. (2019). The Atmospheric River Tracking Method Intercomparison Project (ARTMIP): Quantifying Uncertainties in Atmospheric River Climatology. *Journal of Geophysical Research: Atmospheres*, *124*(24), 13777–13802. https://doi.org/10.1029/2019JD030936 (cit. on p. 23).

Rutz, J. J., & Steenburgh, W. J. (2012). Quantifying the role of atmospheric rivers in the interior western United States. *Atmospheric Science Letters*, *13*(4), 257–261. https://doi.org/10.1002/asl.392 (cit. on p. 11).

Rutz, J. J., Steenburgh, W. J., & Ralph, F. M. (2014). Climatological Characteristics of Atmospheric Rivers and Their Inland Penetration over the Western United States. *Monthly Weather Review*, *142*(2), 905–921. https://doi.org/10.1175/MWR-D-13-00168.1 (cit. on p. 11).

Shields, C. A., Payne, A. E., Shearer, E. J., Wehner, M. F., O'Brien, T. A., Rutz, J. J., Leung, L. R., Ralph, F. M., Marquardt Collow, A. B., Ullrich, P. A., Dong, Q., Gershunov, A., Griffith, H., Guan, B., Lora, J. M., Lu, M., McClenny, E., Nardi, K. M., Pan, M., … Zarzycki, C. (2023). Future Atmospheric Rivers and Impacts on Precipitation: Overview of the ARTMIP Tier 2 High-Resolution Global Warming

Experiment. *Geophysical Research Letters*, *50*(6), e2022GL102091. https://doi.org/10.1029/2022GL102091 (cit. on p. 24).

Shields, C. A., Rosenbloom, N., Bates, S., Hannay, C., Hu, A., Payne, A. E., Rutz, J. J., & Truesdale, J. (2019). Meridional Heat Transport During Atmospheric Rivers in High-Resolution CESM Climate Projections. *Geophysical Research Letters*, *46*(24), 14702–14712. https://doi.org/10.1029/2019GL085565 (cit. on p. 8).

Shields, C. A., Rutz, J. J., Leung, L.-Y., Ralph, F. M., Wehner, M., Kawzenuk, B., Lora, J. M., McClenny, E., Osborne, T., Payne, A. E., Ullrich, P., Gershunov, A., Goldenson, N., Guan, B., Qian, Y., Ramos, A. M., Sarangi, C., Sellars, S., Gorodetskaya, I., ... Nguyen, P. (2018). Atmospheric River Tracking Method Intercomparison Project (ARTMIP): Project goals and experimental design. *Geoscientific Model Development*, *11*(6), 2455–2474. https://doi.org/10.5194/gmd-11-2455-2018 (cit. on pp. 23–25).

Sodemann, H., & Stohl, A. (2013). Moisture Origin and Meridional Transport in Atmospheric Rivers and Their Association with Multiple Cyclones. *Monthly Weather Review*, *141*(8), 2850–2868. https://doi.org/10.1175/MWR-D-12-00256.1 (cit. on pp. 4, 5).

Stohl, A., Forster, C., & Sodemann, H. (2008). Remote sources of water vapor forming precipitation on the Norwegian west coast at 60°N–a tale of hurricanes and an atmospheric river. *Journal of Geophysical Research: Atmospheres*, *113*(D5). https://doi.org/10.1029/2007JD009006 (cit. on pp. 4, 7, 13).

Taylor, K. E., Stouffer, R. J., & Meehl, G. A. (2012). An Overview of CMIP5 and the Experiment Design. *Bulletin of the American Meteorological Society*, *93*(4), 485–498. https://doi.org/10.1175/BAMS-D-11-00094.1 (cit. on p. 25).

Thompson, D. W. J., & Wallace, J. M. (1998). The Arctic oscillation signature in the wintertime geopotential height and temperature fields. *Geophysical Research Letters*, *25*(9), 1297–1300. https://doi.org/10.1029/98GL00950 (cit. on p. 6).

Ullrich, P. A., & Zarzycki, C. M. (2017). TempestExtremes: A framework for scale-insensitive pointwise feature tracking on unstructured grids. *Geoscientific Model Development*, *10*(3), 1069–1090. https://doi.org/10.5194/gmd-10-1069-2017 (cit. on p. 22).

van der Breggen, N. N., & Hudson, P. F. (2024). Influence of atmospheric rivers on extreme rainfall and high streamflow events in northwestern Europe: Rur (Roer) River basin. *Journal of Hydrology: Regional Studies*, *51*, 101644. https://doi.org/10.1016/j.ejrh.2023.101644 (cit. on p. 12).

Viale, M., Valenzuela, R., Garreaud, R. D., & Ralph, F. M. (2018). Impacts of Atmospheric Rivers on Precipitation in Southern South America. *Journal of Hydrometeorology*, *19*(10), 1671–1687. https://doi.org/10.1175/JHM-D-18-0006.1 (cit. on p. 12).

Whan, K., Sillmann, J., Schaller, N., & Haarsma, R. (2020). Future changes in atmospheric rivers and extreme precipitation in Norway. *Climate*

Dynamics, *54*(3), 2071–2084. https://doi.org/10.1007/s00382-019-05099-z (cit. on p. 13).

Wille, J. D., Alexander, S. P., Amory, C., Baiman, R., Barthélemy, L., Bergstrom, D. M., Berne, A., Binder, H., Blanchet, J., Bozkurt, D., Bracegirdle, T. J., Casado, M., Choi, T., Clem, K. R., Codron, F., Datta, R., Battista, S. D., Favier, V., Francis, D., … Zou, X. (2024a). The Extraordinary March 2022 East Antarctica "Heat" Wave. Part I: Observations and Meteorological Drivers. *Journal of Climate*, *37*(3), 757–778. https://doi.org/10.1175/JCLI-D-23-0175.1 (cit. on p. 12).

Wille, J. D., Alexander, S. P., Amory, C., Baiman, R., Barthélemy, L., Bergstrom, D. M., Berne, A., Binder, H., Blanchet, J., Bozkurt, D., Bracegirdle, T. J., Casado, M., Choi, T., Clem, K. R., Codron, F., Datta, R., Battista, S. D., Favier, V., Francis, D., … Zou, X. (2024b). The Extraordinary March 2022 East Antarctica "Heat" Wave. Part II: Impacts on the Antarctic Ice Sheet. *Journal of Climate*, *37*(3), 779–799. https://doi.org/10.1175/JCLI-D-23-0176.1 (cit. on p. 12).

Wille, J. D., Favier, V., Gorodetskaya, I. V., Agosta, C., Kittel, C., Beeman, J. C., Jourdain, N. C., Lenaerts, J. T. M., & Codron, F. (2021). Antarctic Atmospheric River Climatology and Precipitation Impacts. *Journal of Geophysical Research: Atmospheres*, *126*(8), e2020JD033788. https://doi.org/10.1029/2020JD033788 (cit. on p. 12).

Wille, J. D., Favier, V., Jourdain, N. C., Kittel, C., Turton, J. V., Agosta, C., Gorodetskaya, I. V., Picard, G., Codron, F., Santos, C. L.-D., Amory, C., Fettweis, X., Blanchet, J., Jomelli, V., & Berchet, A. (2022). Intense atmospheric rivers can weaken ice shelf stability at the Antarctic Peninsula. *Communications Earth & Environment*, *3*(1), 90. https://doi.org/10.1038/s43247-022-00422-9 (cit. on p. 13).

Yang, Y., Zhao, T., Ni, G., & Sun, T. (2018). Atmospheric rivers over the Bay of Bengal lead to northern Indian extreme rainfall. *International Journal of Climatology*, *38*(2), 1010–1021. https://doi.org/10.1002/joc.5229 (cit. on p. 12).

Zhang, P., Chen, G., Ting, M., Ruby Leung, L., Guan, B., & Li, L. (2023). More frequent atmospheric rivers slow the seasonal recovery of Arctic sea ice. *Nature Climate Change*, *13*(3), 266–273. https://doi.org/10.1038/s41558-023-01599-3 (cit. on p. 13).

Zhu, Y., & Newell, R. E. (1998). A Proposed Algorithm for Moisture Fluxes from Atmospheric Rivers. *Monthly Weather Review*, *126*(3), 725–735. https://doi.org/10.1175/1520-0493(1998)126⟨0725:APAFMF⟩2.0.CO;2 (cit. on pp. 3, 4, 11).

Zou, X., Rowe, P. M., Gorodetskaya, I., Bromwich, D. H., Lazzara, M. A., Cordero, R. R., Zhang, Z., Kawzenuk, B., Cordeira, J. M., Wille, J. D., Ralph, F. M., & Bai, L.-S. (2023). Strong Warming Over the Antarctic Peninsula During Combined Atmospheric River and Foehn Events: Contribution of Shortwave Radiation and Turbulence. *Journal of Geophysical Research: Atmospheres*, *128*(16), e2022JD038138. https://doi.org/10.1029/2022JD038138 (cit. on p. 12).